SI Guide

Manuscript Title Structural basis of ω-3 fatty acid transport across the blood-brain barrier

Author Information Rosemary J. Cater[1], Geok-Lin Chua[2], Satchal K. Erramilli[3], James E. Keener[4], Brendon C. Choy[1], Piotr Tokarz[3], Cheen Fei Chin[2], Debra Q.Y. Quek[2], Brian Kloss[5], Joseph G. Pepe[1], Giacomo Parisi[1], Bernice H. Wong[2], Oliver B. Clarke[1,6], Michael T. Marty[4], Anthony A. Kossiakoff[3], George Khelashvili[7,8*], David L. Silver[2*] & Filippo Mancia[1*]

Table of Contents

Supplementary Notes ……...……. pages 2-3
Supplementary Legend ……...…….……...……..... page 4
Supplementary Figure 1 ……...…….……. page 5

Supplementary Notes

To facilitate analysis of conformational dynamics in our MD simulations, we performed dimensionality reduction analysis on MD trajectories of MFSD2A_GG in a POPC bilayer, with and without LPC-18:1 or LPC-18:3, and in ionic solutions containing either Na^+Cl^- or Li^+Cl^-. From these simulations we extracted several dynamic collective variables (CVs) that quantify: 1) Opening of the IC-gate (residues M182/F399/W403); 2) Widening and hydration of the intracellular cavity; 3) Extent of lysolipid penetration into the intracellular cavity; 4) Penetration of ions from the solution to their interaction sites within the intracellular cavity, including E312 and D92; and 5) Rearrangement of R85 relative to E312 and D88. The MD trajectory frames were projected onto the first two tICA vectors, which represented ~70% of the total dynamics within the system (**Extended Data Fig. 7b**), and the resulting 2D space was divided into 50 discrete microstates using the automated k-means clustering algorithm (**Extended Data Fig. 7a**).

Structural analyses of selected microstates on the tICA landscape (labeled 1-12 in **Extended Data Fig. 7d, f**) describe the major conformational states sampled in the simulations. As revealed by histograms in **Extended Data Fig. 7f**, and from the contributions of each CV to the first two tIC vectors (**Extended Data Fig. 7c**), the first vector (tIC1) mainly describes dynamics of the IC-gate and lysolipid penetration, whereas the second vector (tIC2) predominantly represents dynamics of ion binding. Along tIC2, the 2D space can be divided into regions enriched in conformations where the ion is either bound (Microstates 1-6 in **Extended Data Fig. 7d, f)** or not bound (Microstates 7-12 in **Extended Data Fig. 7d, f**) to the protein. Specifically, Microstates 1-3 describe conformations with an ion bound to E312, whereas Microstates 4-6 correspond to an ensemble of states with an ion bound to D92 (i.e., the Na^+-binding site).

When traversing the tICA space along the tIC1 vector, the system transitions from the states where the IC-gate is closed and lysolipid penetration is negligible, to those where the IC-gate is open, and lysolipid inserts into the cavity (**Extended Data Fig. 7d-f**). In microstates 1, 7, 8, 9, and 10 the IC-gate is closed and no lysolipid penetration is observed. In microstates 2 and 4 the IC-gate widens, and in microstates 3, 5, 6, 11, and 12 the IC-gate is open. These conformational changes allow lysolipid to penetrate, reaching a maximum in microstates 3, 6, and 12. In these three states, the lysolipid headgroup mostly samples the lower region of the cavity and rarely interacts with E312, whereas in microstates 5 and 11, the lysolipid headgroup is predominantly

coordinated by E312 (low P_{lyso} - E312 vertical distance in **Extended Data Fig. 7f** and **Supplementary Video**).

To investigate how different conditions (presence/absence of the lysolipid, ionic solution type) affected sampling of the major structural states described in the main text (**Fig. 3**), we projected our MD trajectory frames onto the 2D tICA space. In the simulations with Li^+Cl^-, the system mostly sampled the upper left part of the tICA landscape (no lysolipid penetration and closed IC-gate), with a number of trajectories (replicates 0 3, 4, 6, 8, and 11) evolving towards Microstate 1, i.e., the ensemble of conformations with ion bound to E312 (**Extended Data Fig. 9a**). Importantly, none of the simulations in this set evolved towards states with ion bound to D92 (microstates 4-6 in **Extended Data Fig. 7d**). Furthermore, simulations initiated upon replacing a POPC adjacent to the open IC-gate with either LPC-18:1 or LPC-18:3 (the location of the trajectory frame in which the replacement was made shown as yellow circle in **Extended Data Fig. 9a**) frequently sampled conformations with the lysolipid headgroup inside the intracellular cavity (lower part of the tICA space; **Extended Data Fig. 9b, c**). Similarly, the simulations initiated from the cryo-EM structure (i.e., with the LPC-18:3 bound within the intracellular cavity), extensively sampled states with the LPC headgroup populating various conformations within the cavity (**Extended Data Fig. 9d**).

Supplementary Table 1 | Raw Single Cell Flow Cytometry Data

Supplementary Video 1 | Molecular dynamics trajectory showing LPC-18:1 exploring the intracellular cavity of MFSD2A. The 18:1 aliphatic tail is coloured in white, whereas the phosphate and the amine groups are coloured in red and blue, respectively. TM5 and TM8 are shown in green, while the gate residues, M182 (on TM5) and W402/F399 (on TM10), are depicted in licorice. E312 and R85 within the central charged region are drawn in surface representation and are coloured in purple. When the LPC-18:1 comes within 4Å of E312 and R85, the colour of the atoms of these residues that become engaged with the lysolipid change from purple to orange. For this video, all 24 MD trajectories with LPC-18:1 were combined into a single trajectory and the resulting trajectory was smoothened using the "smooth" Pymol (Schrödinger) function applied to a window size of 2 (corresponding to a stride of 4ns).

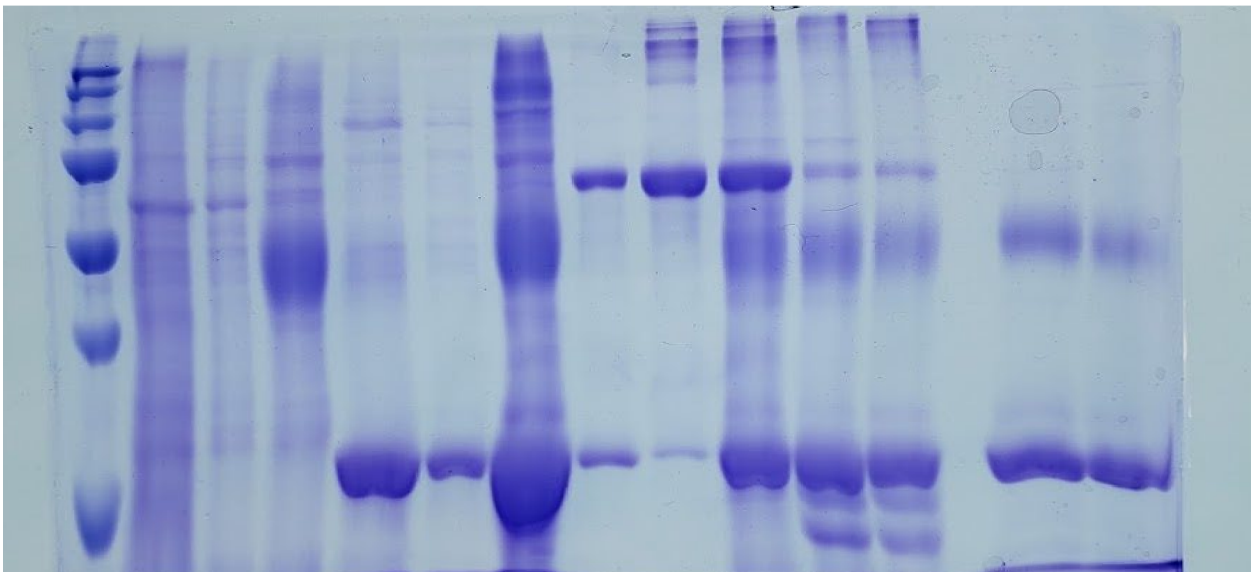

Supplementary Figure 1 | Uncropped gel scan for Extended Data Figure 1f.